Lawrence Berkeley National Laboratory

Title

Dimensional Effects on the Charge Density Waves in Ultrathin Films of TiSe2

Permalink

https://escholarship.org/uc/item/7jv6x4d2

Journal

Nano Letters, 16(10)

ISSN

1530-6984
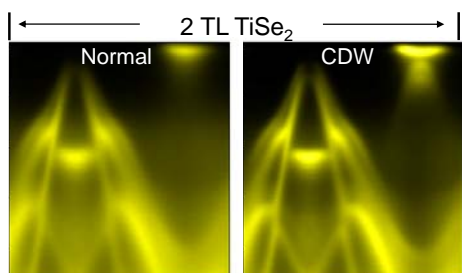
Authors

Chen, P
Chan, Y-H
Wong, M-H
et al.

Publication Date

2016-10-12

DOI

10.1021/acs.nanolett.6b02710

Peer reviewed

Dimensional effects on the charge density waves in ultrathin films of TiSe$_2$

P. Chen,[1,2,3]   Y.-H. Chan,[4]   M.-H. Wong,[1,2]   X.-Y. Fang,[1,2]   M. Y. Chou,[4,5,6] S.-K. Mo,[3] Z. Hussain,[3] A.-V. Fedorov,[3] T.-C. Chiang*[1,2,6]

[1]Department of Physics, University of Illinois at Urbana-Champaign, 1110 West Green Street, Urbana, Illinois 61801-3080, USA

[2]Frederick Seitz Materials Research Laboratory, University of Illinois at Urbana-Champaign, 104 South Goodwin Avenue, Urbana, Illinois 61801-2902, USA

[3]Advanced Light Source, Lawrence Berkeley National Laboratory, Berkeley, California 94720, USA

[4]Institute of Atomic and Molecular Sciences, Academia Sinica, Taipei 10617, Taiwan

[5]School of Physics, Georgia Institute of Technology, Atlanta, GA 30332, USA

[6]Department of Physics, National Taiwan University, Taipei 10617, Taiwan

ABSTRACT: Charge density wave (CDW) formation in solids is a critical phenomenon involving the collective reorganization of the electrons and atoms in the system into a wave structure, and it is expected to be sensitive to the geometric constraint of the system at the nanoscale [1-5]. Here, we study the CDW transition in $TiSe_2$, a quasi-two-dimensional layered material, to determine the effects of quantum confinement and changing dimensions in films ranging from a single layer to multilayers. Of key interest is the characteristic length scale for the transformation from a two-dimensional case to the three-dimensional limit. Angle-resolved photoemission (ARPES) measurements of films with thicknesses up to six layers reveal substantial variations in the energy structure of discrete quantum well states; however, the temperature-dependent band-gap renormalization converges at just three layers. The results indicate a layer-dependent mixture of two transition temperatures and a very-short-range CDW interaction within a three-dimensional framework.

Ultrathin films are basic building blocks for devices; their electronic structure can vary substantially with the addition of each layer in film thickness [6, 7]. The underlying quantum size effects allow property tuning, which can facilitate advanced device applications in the quantum regime [7-9]. While the basic physics of quantum confinement of individual electrons is well-known in terms of the standard picture of a particle in a box, the collective behavior of the coupled electronic and lattice degrees of freedom in connection with CDW formation remains a largely unexplored area [10, 11]. In the present study, we choose $TiSe_2$ for a detailed study.

Despite decades of intense studies of $TiSe_2$, the physics of CDW in this system remains controversial. Our findings of a two-step transition in connection with the crossover from the

two- to three-dimensional behavior should lead to a fundamental rethinking of the underlying CDW interactions in terms of the separation and competition of two- and three-dimensional coupling. Moreover, the basic physics involved in building up a three-dimensional crystal one layer at a time is at the core of nanoscale science and technology; a detailed study of the evolution clarifies the connection between quasiparticle exctitations and the collective behavior of CDWs.

$TiSe_2$ belongs to a vast family of transition metal dichalcognides that make excellent electronic substrate materials beyond graphene. The crystal structure of $TiSe_2$ consists of trilayers (TL) bonded together by van der Waals forces, where each TL is made of a hexagonal Ti atomic layer sandwiched in-between two hexagonal Se atomic layers [12]. The bulk material undergoes a second-order CDW transition at $T_C \sim 205$ K to a commensurate (2x2x2) superlattice [11, 13, 14]; ARPES signatures of the transition include band folding and gap widening, which have been studied extensively in the past [11, 15-17]. Compared to other CDW materials within the same general family, the transition in $TiSe_2$ is particularly simple.

ARPES maps of the band structure of $TiSe_2$ films with thicknesses of $N = 1$-6 TL along the $\bar{\Gamma} - \bar{M}$ direction are presented in Figs. 1a and 1b for the normal phase at 300 K and the CDW phase at 10 K, respectively. These films are grown on a bilayer-graphene-terminated 6H-SiC (0001) surface; the bonding at the interface is expected to be weak and of the van der Waals type, and so substrate effects should be relatively weak [18]. Furthermore, bilayer graphene by itself has a large gap at the zone center and does not yield any photoemission signal that could interfere with the emission from $TiSe_2$. For comparison, the corresponding band structures from first-principles calculations for freestanding $TiSe_2$ films are presented in Figs. 1c and 1d. The concave valence bands centered about $\bar{\Gamma}$ are Se-4p-derived. For the 1-TL film, there are just two bands

reaching close to the Fermi level, which correspond to the Se $4p_{x,y}$ and $4p_z$ states. The convex conduction band centered about $\overline{\mathrm{M}}$ is Ti-$3d$-derived; its bottom reaches just slightly below the Fermi level. As the film thickness increases, additional quantum well states, or subbands, appear. In general, a single band in the 1-TL case should become N subbands for the N-layer film, although some of which might be degenerate, unresolved, or displaying a weak intensity in the experiment [19]. The band multiplication effect is evident in the data, especially at the zone center $\overline{\Gamma}$. For example, the data for 2 TL show an intense quantum well peak at about –1.1 eV, which corresponds well to a quantum well state in the calculation at about –1.3 eV. As the film thickness increases further, more quantum well valence states emerge. Theoretically, the energies of these quantum well states depend sensitively on the boundary conditions. The calculation, assuming freestanding films, does not necessarily predict accurately the experimental energies as the films are grown on a substrate, but the overall evolution of the subbands is consistent with the experiment. The results illustrate a basic feature of ultrathin films: the electronic band structure changes substantially with the addition of each layer. Even at 6-TL, the discreteness of the subbands indicates that the system is far from the bulk limit. For reference, the discreteness of the quantum well states in some thin film systems can be followed to well over one hundred layers [20].

The evolution of the CDW toward the bulk limit is, however, much faster. A prominent feature of CDW formation is the appearance at the $\overline{\mathrm{M}}$ point of a weak replica of the valence bands originally centered at the $\overline{\Gamma}$ point due to (2x2) zone folding as seen in Fig. 1b for all thicknesses. Also, the ARPES maps are sharper for the CDW phase because of reduced thermal broadening at low temperatures. Otherwise, the gross features appear fairly similar for the normal and CDW phases. However, important differences are evident as we focus on the

changes in energy of the valence band maximum and the conduction band minimum. Detailed views of the ARPES maps for 2- and 3-TL films (Fig. 2) show energy shifts of the band extrema between 300 and 10 K that are small compared to the typical energy spacings between quantum well states at the zone center. The fundamental gap, deduced from lineshape fitting to the data, is 54 meV at 300 K and increases to 108 meV at 10 K for the 2-TL film; the corresponding energies for the 3-TL film, 39 and 85 meV, are significantly smaller. In both cases, the system is a small-gap semiconductor at 300 K, and the gap becomes larger at 10 K; the same is true for all of the other thicknesses.

The temperature dependence of the experimentally determined band gap, defined as the energy difference between the valence band top at $\bar{\Gamma}$ and the conduction band bottom at $\bar{M}$, reveals the CDW transition (Fig. 3). For each film thickness, the gap remains a constant upon decreasing temperature from 300 K until the sample reaches around 200 K, below which the gap increases; the onset marks the CDW transition. A comparison of the curves shows that the onset behavior is the same, within experimental error, for $N = 3$-6. The $N = 1$ film shows a CDW onset at a substantially higher temperature of $T_{C1} \sim 232$ K as reported previously and indicated by the green vertical line in Fig. 3a [5]. The $N = 2$ case shows two onsets, one at the same T_{C1} and another at $T_{C2} \sim 205$ K, as indicated by the green and blue vertical lines, respectively, in Fig. 3b. For $N = 3$-6, each data set can be well described by a single onset at T_{C2}, but there also appears a very small tail with a very weak onset at T_{C1}. This tail between T_{C2} and T_{C1} is just about the size of the error bar, but it is consistently seen for all thicknesses in the range of $N = 3$-6, and so it is included in our analysis.

The red fitting curves in Fig. 3 are fits based on the semi-phenomenological BCS gap equation:

$$\Delta^{2}\left(T\right)-\Delta^{2}\left(T_{\mathrm{C}}\right) \propto \tanh^{2}\left(A\sqrt{\frac{T_{\mathrm{C}}}{T}-1}\right) \qquad (1)$$

where A is a proportional constant. The right-hand side reduces to a linear function near the transition temperature T_{C}. The fits consist of a linear combination of two transitions, one at T_{C1} and the other at T_{C2}, except for $N = 1$, which shows just one onset at T_{C1}. The data for N = 3-6 could be fit almost as well with just one onset at T_{C2} without including the very weak onset at T_{C1}. The percentage of the onset at T_{C1} from the fitting (Fig 4a) converges rapidly to about 10% at N = 3 and beyond. The red dashed curve is an exponential fit with a damping length of 0.8 TL. The results indicate a very rapid approach to the bulk limit.

The limiting energy gaps at 300 and 10 K are extracted from the ARPES data (Fig 4b). The gap for the CDW phase at 10 K is larger than that for the normal phase at 300 K by about 40-55 meV across the different thicknesses. For both phases, the gap becomes larger at smaller thicknesses; this trend is consistent with the general tendency of a larger gap with increasing degree of quantum confinement. The dashed curves are exponential fits to the data; the characteristic decay lengths are 0.7 and 1.0 TL for the normal and CDW phases, respectively. Again, the bulk limit is reached very quickly. The band structures from first-principles calculations (Figs. 1c and 1d) also show a rapid variation of the band gaps. Plotted in Figs. 4c and 4d for direct comparison are the normalized variations of the gaps for both the normal and CDW phases; the experimental and theoretical results are very similar, but the decay lengths from experiment are somewhat shorter than the theoretical results. We do not have a specific explanation for the less than perfect agreement, but some discrepancies between experiment and theory are not uncommon even for the best theoretical methods available today.

The significant mixture of two transitions at T_{C1} and T_{C2} for $N = 2$ is a phenomenon never

seen before in this type of dimensional crossover behavior associated with phase transitions. The implication is a very-short-range effective interaction among the layers of $TiSe_2$. The physical picture is that each layer undergoes a (2x2) transition independently at the higher transition temperature T_{C1}, which is also the transition temperature of a single layer. At the lower transition temperature T_{C2}, the two (2x2) layers lock their structures into a (2x2x2) anti-phase stack, which is also the transition temperature at larger N values including the bulk limit. Thus, just two layers are sufficient to exhibit a bulklike transition; based on the red fitting curve in Fig. 4a, the $N = 3$ film should be indistinguishable, within experimental error, from the bulk limit. The energy gaps are also fully convergent at $N = 3$ (Fig. 4b).

The evolution of the subband structure seen in Fig. 1 suggests that films of $TiSe_2$ will need to be very thick, perhaps up to tens of layers, before the discreteness of the subbands becomes sufficiently smeared out by thermal and lifetime effects to yield a bulklike density of states. Yet the CDW transition converges extremely rapidly. This apparently puzzling effect can be understood as a result of the limited ranges in energy and momentum of the CDW interaction. The CDW transition mainly involves electronic states that lie within a narrow energy range across the gap as represented by the top portion of the highest valence subband and the bottom portion of the lowest conduction subband. The energy dispersion relations of these subbands elsewhere in the Brillouin zone and of the other subbands away from the Fermi level are insensitive to the atomic distortion associated with the CDW transition and do not contribute significantly to the changing energetics of the system. Therefore, the discrete subbands away from the Fermi level are just bystanders of the CDW transition.

Building up a three-dimensional crystal one layer at a time is a powerful approach for materials synthesis and for unveiling dimensional effects. For the CDW transition in $TiSe_2$, our

layer-resolved ARPES results indicate that the transition develops a bulk character already if each TiSe$_2$ layer has at least one neighboring layer. This happens at just two layers, and the implication is that the x2 stacking order is governed by essentially a nearest-neighbor-only interaction. The very short range of the interaction nevertheless leads to a robust three-dimensional CDW order. It is conceivable that the same physics might be at play for other transition metal dichalcogenides, many of which show CDW transitions despite their diverse electronic properties (metals, semimetals, or semiconductors) and different symmetry properties (commensurate or incommensurate transitions). Layer-resolved spectroscopic studies, as demonstrated in this work, will be a powerful tool for extracting the properties of the underlying CDW and other interactions and for elucidating the transformation from two- to three-dimensional behavior.

Materials and Methods

Multilayer thin films of TiSe$_2$ were grown *in situ* in the molecular beam epitaxy (MBE) and photoemission systems at beamlines 12.0.1 and 10.0.1, Advanced Light Sources, Lawrence Berkeley National Laboratory. Substrates of 6H-SiC(0001) were flash-annealed for multiple cycles to form a well-ordered bilayer graphene on the surface which is ideal for van der Waals epitaxial growth [18]. The films were grown by co-evaporating high-purity Ti and Se from an electron-beam evaporator and a Knudsen effusion cell, respectively, onto a substrate maintained at 350 °C. The growth process was monitored by reflection-high-energy-electron diffraction (RHEED) and the growth rate was set to 30 minutes per single layer of TiSe$_2$.

ARPES measurements were performed at a base pressure of ~3×10^{-11} mbar with linearly polarized light. The system energy resolution was less than 20 meV, and the angular resolution was 0.2°. The crystallographic orientation of each sample was determined by RHEED and, more

precisely, from constant-energy-contour ARPES mapping to identify the high symmetry points in k space. A number of photon energies were used in the experiment to yield a high photoemission intensity for the portion of the bands of interest. The photon energies used were 58, 67, and 46 eV for the data centered about $\bar{\Gamma}$ for the normal phase, $\bar{\Gamma}$ for the CDW phase, and $\bar{M}$ for both phases, respectively. We also experimented with the effects of changing photon polarization; the Se $4p$ band top shows a stronger photoemission intensity with s-polarized light, which permits a more accurate determination of the band dispersion.

First-principles calculations were performed using the Vienna *ab initio* package (VASP) [21-23] with the projector augmented wave method [24, 25]. The multilayer system was simulated with a 17-Å vacuum region in order to suppress the interaction between adjacent layers. A plane wave energy cut-off of 320 eV and an 18x18x1 k-mesh were employed. The generalized gradient approximation with the Perdew-Burke-Ernzerhof (PBE) functional [26] was used for structural optimization of monolayer TiSe$_2$; the resulting lattice constant, 3.538 Å, is very close to the experimental in-plane lattice constant in the bulk. The PBE functional is known to overestimate the interlayer distance for multilayers. We fixed the in-plane lattice constant and applied the van der Waals correction with the DFT-D3 method [27] to optimize the interlayer distance. For comparison, the calculated lattice constants, $a = 3.522$ Å and $c = 6.017$ Å, for bulk TiSe$_2$ based on the DFT-D3 method are in excellent agreement with experimental values. The calculation shows that the CDW phase has a lower energy at $T = 0$ for all film thicknesses. The electronic energy bands of the films shown in Fig. 1 were calculated with the optimized structures for the films using the GGA + U method [28], with the parameter $U = 6.5$ determined from a fit to the bilayer band structure obtained using the hybrid HSE functional [29].

ASSOCIATED CONTENT

Supporting information

Experimental and analysis details, and additional figures. This material is available free of charge via the Internet at http:// pubs.acs.org.

AUTHOR INFORMATION

Corresponding Author

*E-mail: tcchiang@illinois.edu.

Author Contributions

PC with the aid of MHW, XYF, SKM, ZH, AVF, and TCC performed MBE growth, ARPES measurements, and data analysis. YHC and MYC performed first-principles calculations. PC and TCC wrote the paper. TCC, PC, and MYC interpreted the data. TCC and AVF jointly led the experimental project.

Notes

The authors declare no competing financial interest.

REFERENCES

1. Gerber, S.; Jang, H.; Nojiri, H.; Matsuzawa, S.; Yasumura, H.; Bonn, D. A.; Liang, R.; Hardy, W. N.; Islam, Z.; Mehta, A.; Song, S.; Sikorski, M.; Stefanescu, D.; Feng, Y.; Kivelson, S. A.; Devereaux, T. P.; Shen, Z.-X.; Kao, C.-C.; Lee, W.-S.; Zhu, D.; Lee, J.-S. *Science* **2015**, 350, 949–952.

2. Xi, X.; Zhao, L.; Wang, Z.; Berger, H.; ForrÓ, L.; Shan, J.; Mak, K. *Nature Nanotech.* **2015**, 10, 765–769.

3. Hajiyev, P.; Cong, C.; Qiu, C.; Yu, T. *Sci. Rep.* **2013**, 3, 2593.

4. Peng, J.-P.; Guan, J.-Q.; Zhang, H.-M.; Song, C.-L.; Wang, L.; He, K.; Xue, Q.-K.; Ma, X.-C. *Phys. Rev. B* **2015**, 91, 121113.

5. Chen, P.; Chan, Y.-H.; Fang, X.-Y.; Zhang, Y.; Chou, M. Y.; Mo, S.-K.; Hussain, Z.; Fedorov, A.-V.; Chiang, T.-C. *Nat. Commun.* **2015**, 6, 8943.

6. Zhang, Y.; He, K.; Chang, C.-Z.; Song, C.-L.; Wang, L.-L.; Chen, X.; Jia, J.-F.; Fang, Z.; Dai, X.; Shan, W.-Y.; Shen, S.-Q.; Niu, Q.; Qi, X.-L.; Zhang, S.-C.; Ma, X.-C.; Xue, Q.-K. *Nature Phys.* **2010**, 6, 584–588.

7. Wang, Q. H.; Kalantar-Zadeh, K.; Kis, A.; Coleman, J. N.; Strano, M. S. *Nat. Nanotechnol.* **2012**, 7, 699–712.

8. Radisavljevic, B.; Radenovic, A.; Brivio, J.; Giacometti, V.; Kis, A. *Nat. Nanotechnol.* **2011**, 6, 147–150.

9. Jariwala, D.; Sangwan, V. K.; Lauhon, L. J.; Marks, T. J.; Hersam, M. C. *ACS Nano* **2014**, 8, 1102–1120.

10. Wilson, J. A.; DiSalvo, F. J.; Mahajan, S. *Adv. Phys.* **1975**, 24, 117-201.

11. Rossnagel, K. *J. Phys. Condens. Matter* **2011**, 23, 213001.

12. Rossnagel, K. *New J. Phys.* **2010**, 12, 125018.

13. Di Salvo, F. J.; Moncton, D. E.; Waszczak, J. V. *Phys. Rev. B* **1976**, 14, 4321.

14. Holt, M.; Zschack, P.; Hong, H.; Chou, M. Y.; Chiang, T.-C. *Phys. Rev. Lett.* **2011**, 86, 3799.

15. May, M. M.; Brabetz, C.; Janowitz, C.; Manzke, R. *Phys. Rev. Lett.* **2011**, 107, 176405.

16. Cercellier, H.; Monney, C.; Clerc, F.; Battaglia, C.; Despont, L.; Garnier, M. G.; Beck, H.; Aebi, P.; Patthey, L.; Berger, H.; Forró, L. *Phys. Rev. Lett.* **2007**, 99, 146403.

17. Kidd, T. E.; Miller, T.; Chou, M. Y.; Chiang, T.-C. *Phys. Rev. Lett*. **2002**, 88, 226402.

18. Wang, Q. Y.; Zhang, W. H.; Wang, L. L.; He, K.; Ma, X. C.; Xue, Q. K. *J. Phys.: Condens. Matter* **2013**, 25, 095002.

19. Chiang, T.-C. *Surf. Sci. Rep.* **2000**, 39, 181–235.

20. Paggel, J. J.; Miller, T.; Luh, D.-A.; Chiang, T.-C. *Appl. Surf. Sci*. **2000,** 162-163, 78-85.

21. Kresse, G.; Hafner, J. *Phys. Rev. B* **1993**, 48, 13115-13118.

22. Kresse, G.; Furthmüller, J. *Comput. Mater. Sci.* **1996**, 6, 15-50.

23. Kresse, G.; Furthmüller, J. *Phys. Rev. B* **1996**, 54, 11169-11186.

24. Blöchl, P. E. *Phys. Rev. B* **1994**, 50, 17953.

25. Kresse, G.; Joubert, J. *Phys. Rev. B* **1999**, 59, 1758.

26. Perdew, J. P.; Burke, K.; Ernzerhof, M. *Phys. Rev. Lett.* **1996**, 77, 3865.

27. Grimme, S.; Antony, J.; Ehrlich, S.; Krieg, S. *J. Chem. Phys.* **2010**, 132, 154104.

28. Dudarev, S. L.; Botton, G. A.; Savrasov, S. Y.; Humphreys, C. J.; Sutton, A. P. *Phys. Rev. B* **1998**, 57, 1505.

29. Heyd, J.; Scuseria, G. E.; Ernzerhof, M. *J. Chem. Phys.* **2003,** 118, 8207.

Fig. 1. Electronic band structure of TiSe$_2$ thin films. ARPES maps of TiSe$_2$ thin films with thicknesses ranging from 1 [5] to 6 TL along the $\overline{\Gamma}\overline{M}$ direction for (**a**) the normal phase at 300 K and (**b**) the CDW phases at 10 K. Data were taken with *p*-polarized light at 58 eV. Corresponding calculated band structures are shown for the normal phase in (**c**) for the CDW phase in (**d**).

Fig. 2. Band gaps in TiSe$_2$ films. Detailed ARPES maps for 2- and 3-TL TiSe$_2$ in the (**a**) normal and (**b**) CDW phases. The data at $\overline{\Gamma}$ and $\overline{M}$ were taken with *s*- and *p*-polarized light, respectively. The energies of the band edges obtained from curve fitting are indicated. The photon energies used were 58, 46, 58, and 46 eV, respectively for the four cases in (**a**) and 67, 46, 67, and 46 eV, respectively, for the four cases in (**b**).

Fig. 3. Temperature dependence of band gaps and transition temperatures. The measured energy gap squared as a function of temperature for (**a**) 1 TL [5], (**b**) 2 TL, (**c**) 3 TL, and (**d**) 6 TL. The energy gap is the difference between the valence band top at $\overline{\Gamma}$ and the conduction band bottom at $\overline{M}$, measured with 58 and 46 eV photons, respectively. The red curves are fits using a BCS-type gap equation. Two transition temperatures T_{C1} and T_{C2} are indicated by blue and greens dashed lines, respectively.

Fig. 4. Evolution of the character of the transition and band gaps with film thickness. (**a**) The percentage of the weight of the onset at T_{C1} for different thicknesses. It is 100% for a single layer but reduces to about 10% for $N = 3$-6. The dashed curve is an exponential fit. (**b**) Energy gap as a function of film thickness in the normal (CDW) phase measured with 58 (67) and 46 (46) eV photons for the $\overline{\Gamma}$ and $\overline{M}$ band edges, respectively. The curves are exponential fits. (**c**) Normalized normal-phase energy gaps as a function of film thickness from experiment and

theory. (**d**) Normalized CDW energy gaps as a function of film thickness from experiment and

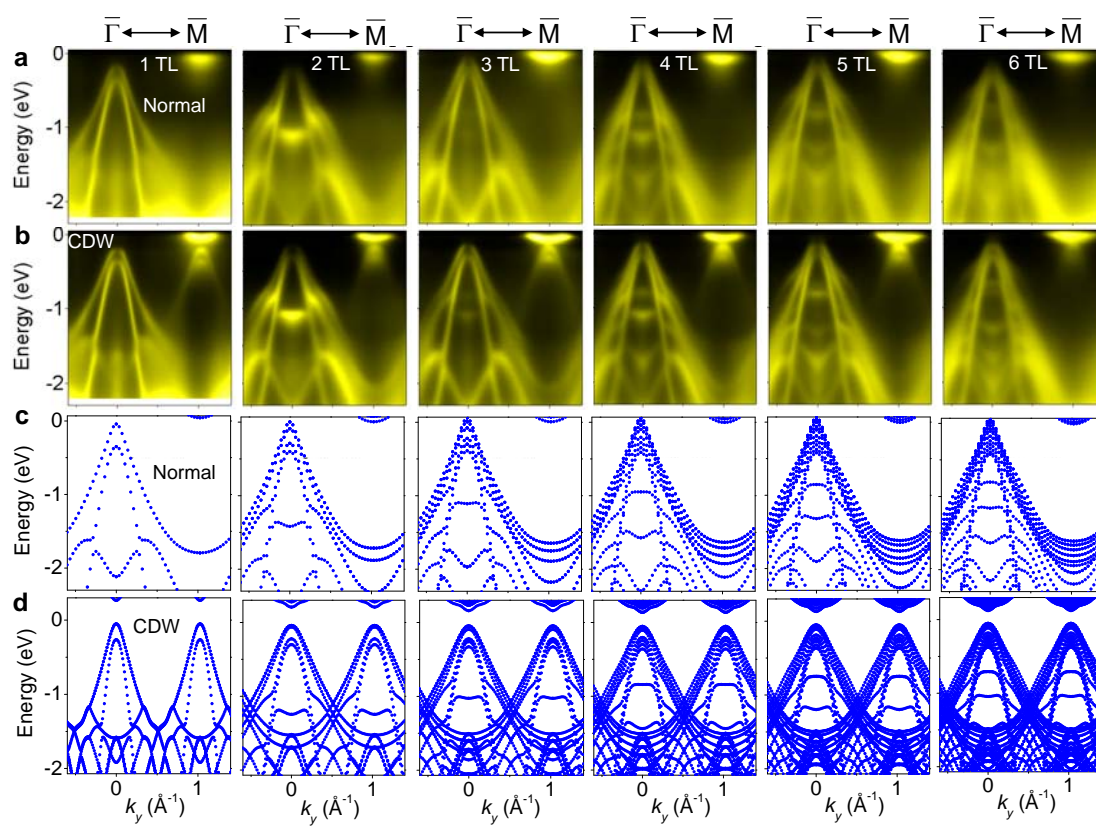theory. The results for bulk TiSe$_2$ ($N = \infty$) are taken from an earlier study [5].
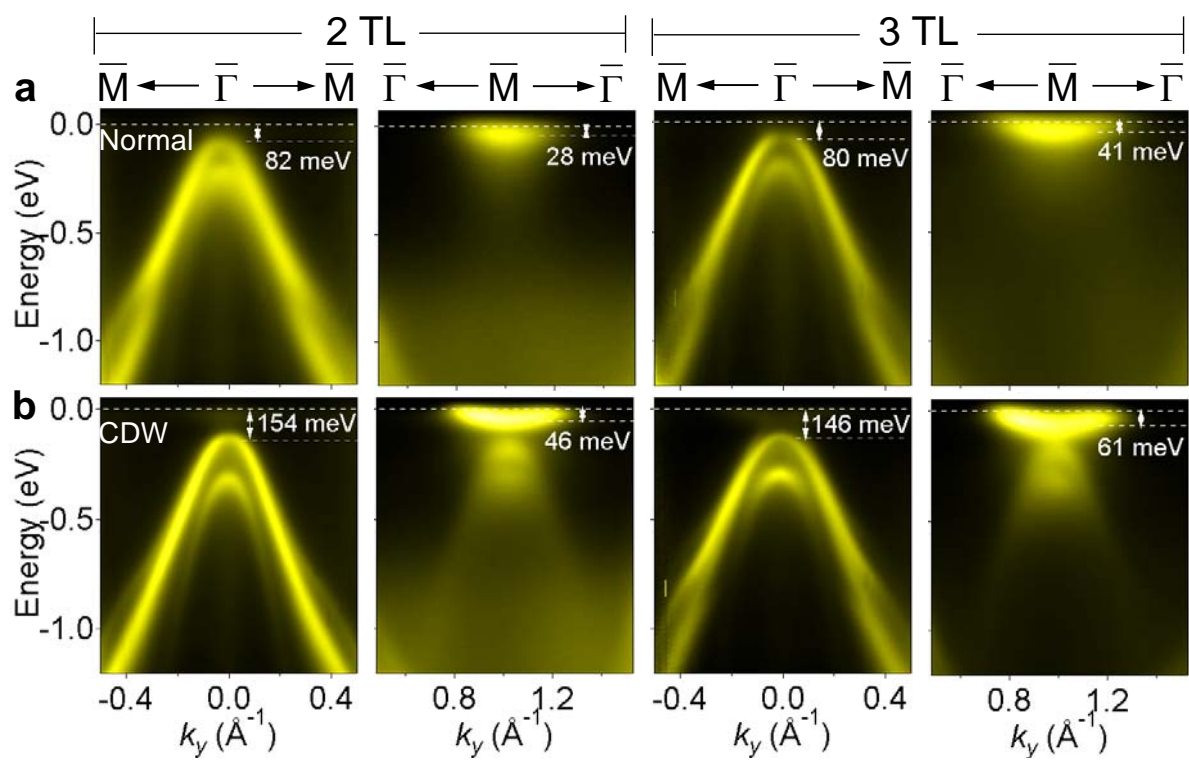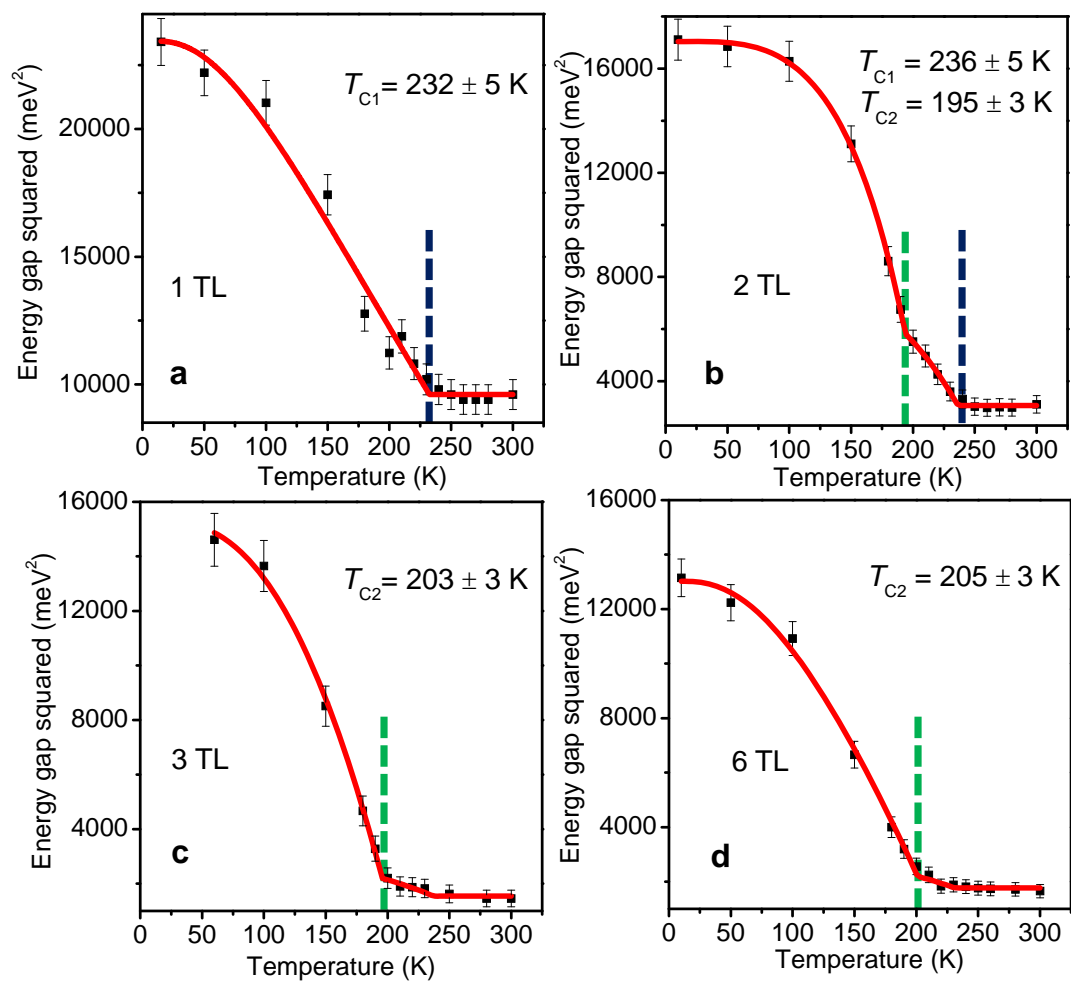
Fig. 1

Fig. 2

Fig. 3

Fig. 4